

Hemispheric Image Modeling and Analysis Techniques for Solar Radiation Determination in Forest Ecosystems

Ellen Schwalbe, Hans-Gerd Maas, Manuela Kenter, and Sven Wagner

Abstract

Hemispheric image processing with the goal of solar radiation determination from ground-based fisheye images is a valuable tool for silvicultural analysis in forest ecosystems. The basic idea of the technique is taking a hemispheric crown image with a camera equipped with a 180° fisheye lens, segmenting the image in order to identify solar radiation relevant open sky areas, and then merging the open sky area with a radiation and sun-path model in order to compute the total annual or seasonal solar radiation for a plant. The results of hemispheric image processing can be used to quantitatively evaluate the growth chances of ground vegetation (e.g., tree regeneration) in forest ecosystems.

This paper shows steps towards the operationalization and optimization of the method. As a prerequisite to support geometric handling and georeferencing of hemispheric images, an equi-angular camera model is shown to describe the imaging geometry of fisheye lenses. The model is extended by a set of additional parameters to handle deviations from the ideal model. In practical tests, a precision potential of 0.1 pixels could be obtained with off-the-shelf fisheye lenses. In addition, a method for handling the effects of chromatic aberration, which may amount to several pixels in fisheye lens systems, is discussed. The central topic of the paper is the development of a versatile method for segmenting hemispheric forest crown images. The method is based on linear segment-oriented classification on radial profiles. It combines global thresholding techniques with local image analysis to ensure a reliable segmentation in different types of forest under various cloud conditions. Sub-pixel classification is incorporated to optimize the accuracy of the method. The performance of the developed method is validated in a number of practical tests.

Introduction

Forest ecosystems are characterized by a rather specific solar radiation situation. In dense forests, solar radiation is one of the critical parameters determining the growth chances of ground vegetation, e.g., in tree regeneration (Burschel and Schmaltz, 1965; Pacala *et al.*, 1994). Therefore, there is a

need for efficient methods for measuring solar radiation in silviculture research. On-site solar radiation measures, which are representative for the whole growth period of a tree, must be acquired at pre-defined locations. A standard technique to determine growth-relevant solar radiation in forest ecosystems is based on photosynthetically active radiation (PAR) sensors. PAR sensors deliver an integral measure on the radiation in the photosynthetic relevant spectrum. Their sensitivity corresponds to the spectral efficiency of chlorophyll. The development conditions of young plants at a certain location can be determined by extrapolation schemes applied to time series of PAR sensor measurements.

An efficient alternative to time consuming PAR sensor time series is given by hemispheric photography. This method allows for a determination of the solar radiation situation from a single photo. The basic idea of the technique is taking a hemispheric crown image in a forest ecosystem with a camera equipped with a 180° fisheye lens, segmenting the image in order to identify solar radiation-relevant open sky areas, and then merging the open sky area with a radiation model and a sun-path model in order to compute the total annual or seasonal solar radiation for a plant (Figure 1). While PAR sensors deliver only a scalar radiation measure, hemispherical images offer the advantage of providing spatially resolved radiation-relevant information on the whole hemisphere from a single image.

Hemispherical photography using 180° fisheye lenses has first been used to evaluate the radiation conditions in forest stands for the determination of site-related factors for young plants in the late-1950s (Evans and Coombe, 1959). Many attempts have been undertaken to develop reliable forest crown image segmentation techniques: a manual technique on analogue photography has been presented by Anderson (1964). A first step into automated image processing was shown by Bonhomme and Chartier (1972). Techniques for computerized analysis were shown by Olsson *et al.* (1982) for analogue imagery and by Englund *et al.* (2000) for digital imagery. Up to now, interactive global thresholding is still the most common segmentation method.

Ellen Schwalbe and Hans-Gerd Maas are with the Institute of Photogrammetry and Remote Sensing, Technische Universität Dresden, Helmholtzstraße 10, 01062 Dresden, Germany (ellen.schwalbe@tudresden.de).

Manuela Kenter and Sven Wagner are with the Institute of Silviculture and Forest Protection, Technische Universität Dresden, Pienner Str. 8, 01737 Tharandt, Germany.



Figure 1. Hemispheric forest crown image, projected sun path (schematic sketch not at scale).

In the following, we will show a refined method of determining growth-relevant solar radiation measures from high-resolution digital hemispheric images. The next section will briefly address data acquisition, followed by a geometric model for fisheye lens cameras and a calibration tool developed as a prerequisite for geometric image measurements. Next, an optimized automatic image segmentation technique is introduced which considers and exploits the special characteristics of hemispheric forest crown images. The method allows for a sub-pixel classification of open sky regions in the hemisphere. The final section shows results of practical studies and a comparison between the results of PAR sensor measurements and hemispheric photography.

Hemispheric Forest Crown Image Acquisition

Hemispheric forest crown imaging has long been based on analogue photography (Dohrenbusch, 1989; Wagner, 1998). Analogue photography requires film processing and scanning, limiting both the efficiency of the method and the reproducibility of results. Digital photography has been applied since the early 1990s (e.g., Chen *et al.*, 1991). The use of a high-resolution digital stillvideo camera removes the disadvantages of analogue film and allows for rather efficient photogrammetric solar radiation data acquisition.

The images shown in this paper were taken by a high-resolution digital camera with a 4,500 pixel \times 3,000 pixel Bayer pattern RGB CMOS sensor, equipped with a 180° full circle fisheye lens. The camera is placed on the forest ground with the optical axis pointing upward for taking hemispheric crown images. In order to allow an intersection of the image with astronomical sun path parameters, the camera has to be leveled and north-oriented. The exposure settings were measured above canopy with an opening angle of 7.5° (Wagner 1998, Clearwater *et al.*, 1999). This “above canopy reference method” (Zhang *et al.*, 2005) relates exposure

settings to unobscured sky by adding one *f*-stop. The photos were taken under 70 to 90 percent cloudiness to prove the potential of the method to be applied not only under clear sky or homogeneously overcast conditions.

To prepare the images for solar radiation analysis, two tasks have to be solved. The first task is the geometric modeling and calibration of the fisheye lens camera system in order to obtain the geometric registration between image plane and object space. The second and main task is the segmentation and classification of hemispherical canopy images. Sub-pixel precision in the classification process may be crucial to optimize the results of the technique in dark forest environments with less than 5 percent radiation-relevant crown gap area.

Fisheye Camera Calibration

Fisheye lenses with an opening angle of 180° or more are often used for visualization tasks such as the documentation of ceiling frescos in historical buildings or internet presentations of building interiors. Beyond these pure visualization tasks, fisheye lenses may be an interesting tool for photogrammetric measurement systems. Fisheye lenses are, for instance, being used in mobile mapping systems (van den Heuvel *et al.*, 2006). Their suitability for hemispheric image acquisition in solar radiation analysis is obvious. In the following, a fundamental geometric model for photogrammetric handling of fisheye lens images based on an equi-angular camera model will be developed. This model will be extended by additional parameters to encounter effects of lens distortion. Special attention will be paid to chromatic aberration effects, which are typical for fisheye lenses.

Equi-angular Camera Model

The imaging geometry of fisheye lenses deviates considerably from the standard central perspective model. Fisheye lenses are often modeled on the basis of an equi-angular camera model (Ray, 1994).

The basic geometry of an equi-angular camera model is shown in Figure 2. To derive the observation equations (in analogy to the collinearity equations for central perspective imagery), we first transform the object coordinates into the camera coordinate system using the following transformation equations:

$$\begin{aligned} X_C &= a_{11} \cdot (X - X_0) + a_{21} \cdot (Y - Y_0) + a_{31} \cdot (Z - Z_0) \\ Y_C &= a_{12} \cdot (X - X_0) + a_{22} \cdot (Y - Y_0) + a_{32} \cdot (Z - Z_0) \\ Z_C &= a_{13} \cdot (X - X_0) + a_{23} \cdot (Y - Y_0) + a_{33} \cdot (Z - Z_0) \end{aligned} \quad (1)$$

where X_C, Y_C, Z_C = object point coordinates in the camera coordinate system, X, Y, Z = object point coordinates in the object coordinate system, X_0, Y_0, Z_0 = coordinates of the projection center, and a_{ij} = elements of the rotation matrix

The equi-angular camera model postulates that the relation between the angle of incidence of an object point and the resulting radial distance of an image point to the principle point is constant. Consequently, the following equation can be set up as basic equation for the fisheye projection:

$$\frac{\alpha}{r} = \frac{90^\circ}{R} \quad r = \sqrt{x'^2 + y'^2} \quad (2)$$

where α = angle of incidence, r = distance between image point and optical axis, R = image radius, and x', y' = image coordinates.

The angle of incidence α is defined by the coordinates of an object point X, Y, Z and the exterior orientation

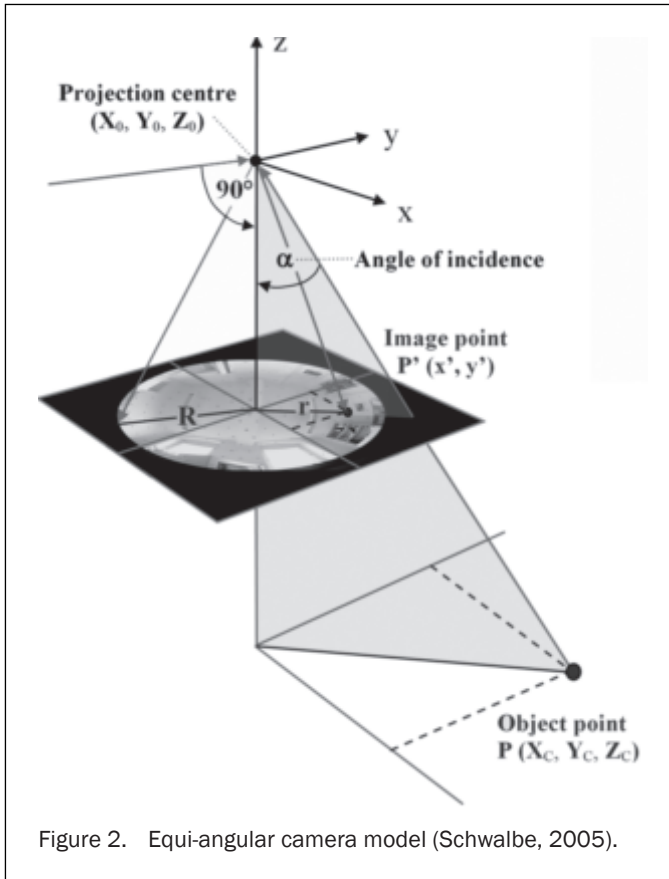


Figure 2. Equi-angular camera model (Schwalbe, 2005).

parameters. The image radius R replaces the principle distance of the central perspective projection model as a scale factor. In Equation 2, the image coordinates x' and y' are still included in the radius r . To obtain separate equations for the two image coordinates, we make use of the coplanarity of an object point, its corresponding image point, and the z -axis of the camera coordinate system. Based on the intercept theorem, we can set up the following equation:

$$\frac{x'}{y'} = \frac{X_C}{Y_C} \quad (3)$$

where X_C, Y_C = object point coordinates in the camera coordinate system, and x', y' = image coordinates.

After some transformations of the above equations, the final fisheye projection observation equations are obtained:

$$x' = \frac{\frac{2 \cdot R}{\pi} \cdot \arctan\left(\frac{\sqrt{(X_C)^2 + (Y_C)^2}}{Z_C}\right)}{\sqrt{\left(\frac{Y_C}{X_C}\right)^2 + 1}} + dx + x_H \quad (4)$$

$$y' = \frac{\frac{2 \cdot R}{\pi} \cdot \arctan\left(\frac{\sqrt{(X_C)^2 + (Y_C)^2}}{Z_C}\right)}{\sqrt{\left(\frac{X_C}{Y_C}\right)^2 + 1}} + dy + y_H$$

where x', y' = image coordinates, X_C, Y_C, Z_C = object point coordinates in the camera coordinate system (Equation 4),

R = image radius, x_H, y_H = coordinates of the principle point, and d_x, d_y = distortion terms.

These observation equations describe the projection of an object point onto the image plane for a fisheye lens. They are extended by two terms d_x, d_y to cover lens distortion and other systematic deviations from the ideal equi-angular model.

Self-calibration Parameters

We adopted the five-parameter model, which was introduced into photogrammetry for handling lens distortion of central perspective images by Brown (1971), to model radial and decentering distortion of fisheye lenses. The analysis of a number of practical experiments showed, that these parameters are well-suited to model lens distortion effects of fisheye lenses in an equi-angular camera model. In addition, the coordinates of the principle point (x_H, y_H) and the fisheye image radius R are introduced as unknowns. Effects of the A/D conversion of the images may be handled by introducing two parameters of an affine transformation (x' -scale and shear; El-Hakim, 1986).

$$dx = x' \cdot (A_1 r^2 + A_2 r^4 + A_3 r^6) + B_1 \cdot (r^2 + 2x'^2) + 2B_2 x' y' + C_1 \cdot x' + C_2 \cdot y \quad (5)$$

$$dy = y' \cdot (A_1 r^2 + A_2 r^4 + A_3 r^6) + 2B_1 x' y' + B_2 \cdot (r^2 + 2y'^2) \quad (5)$$

$$r = \sqrt{x'^2 + y'^2}$$

where A_1, A_2, A_3 = radial distortion parameters, B_1, B_2 = decentering distortion parameters, and C_1, C_2 = horizontal scale factor, shear factor.

The mathematical model of equi-angular projection (Equation 4), extended by additional parameters to reflect the physical reality of the imaging system (Equation 5), can be implemented as a module into spatial resection, spatial intersection, and bundle adjustment. It can also be used to derive epipolar lines in stereoscopic hemispheric image processing. Schwalbe and Schneider (2005) show the combination of the hemispheric camera model with a panoramic camera model (Schneider and Maas, 2006) to handle full-spheric $360^\circ \times 180^\circ$ imagery generated by a fisheye lens on a rotating linear array imaging device.

Practical results obtained from the camera model are shown by Schwalbe (2005). Validation images were taken in a fisheye camera calibration cell established at Dresden University of Technology (Figure 3). Typical results of a fisheye

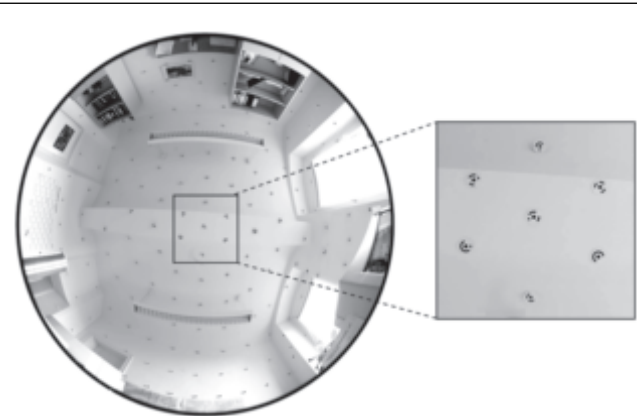


Figure 3. Fisheye camera calibration cell at Dresden University of Technology.

TABLE 1. CAMERA CALIBRATION RESULTS: INFLUENCE OF ADDITIONAL PARAMETERS ON σ_0

Estimated Parameters	σ_0 [pixel]
with exterior orientation only ($X_0, Y_0, Z_0, \omega, \varphi, \kappa$)	9.540
with interior orientation additionally (R, x_H, y_H)	8.781
with radial-symmetric distortion additionally (A1, A2, A3)	0.117
with radial-asymmetric and tangential distortion additionally (B1, B2)	0.098
with affinity and shear additionally (C1, C2)	0.096

camera calibration are listed in Table 1. A standard deviation of unit weight $\sigma_0 = 0.1$ pixel could be obtained from a spatial resection. As a dominating effect, the introduction of the radial symmetric distortion parameters could improve the precision by a factor of 80. The residual image obtained from a spatial resection based on the equi-angular camera model with the additional parameters showed no remaining systematic effects. The precision potential achieved in this test is a bit worse than the precision which is usually obtained from digital central perspective camera systems in industrial applications. A major factor preventing a higher precision was posed by the precision of the reference coordinates of the calibration field itself. However, the precision is more than adequate for the task of solar radiation analysis.

A second test with a low-cost fisheye lens (Schwalbe and Maas, 2006) showed rather similar results. The fact that no more systematic effects could be seen in the residual image suggests that fisheye images can be treated in self-calibration in the same way as central perspective images, if the collinearity equation is replaced by the observation equation of the equi-angular model in the core software modules.

Handling of Chromatic Aberration

A thorough analysis of the image quality of hemispheric images generated by fisheye lenses shows chromatic aberration effects, which are clearly visible as color seams in the image towards the boundaries of the image. The seams may be more than a pixel wide and lead to a mis-registration between the RGB channels of the image, which interferes in an unpredictable manner with the Bayer-pattern sensor. This will severely deteriorate the results of pixel-based multi-spectral classification techniques. Similar effects have been reported by Luhmann *et al.* (2006) and by van den Heuvel *et al.* (2006).

Due to the radial symmetric character of chromatic aberration, the effect can be compensated by a channel-

variant calibration procedure. The basic idea of the procedure is to take a calibration field image, process the three color channels separately, perform a spatial resection with one common parameter set for exterior and interior orientation, but individual radial lens distortion parameters for each color channel and then to resample the red and blue channel onto the geometry of the green channel using these distortion parameters (Schwalbe and Maas, 2006).

Table 2 shows the results of a fisheye camera calibration with channel-variant radial distortion parameters. The calibration cell color images (Figure 3) were split into their RGB channels. The image coordinates of the targets were determined in each channel separately. The spatial resection was performed for the three channels together, introducing one common parameter set for exterior orientation, interior orientation and affine distortion parameters, and three channel-variant sets of parameters for radial lens distortion. Image coordinate differences of up to three pixels were determined between the channels. Surprisingly, the differences between the red and green channels were much larger than the differences between the green and blue channel.

Based on the results of the channel-specific calibration, the images can be resampled into a common geometry at a precision in the order of 0.1 pixel. The success of this approach is, however, partly compromised by some edge-crisping, which is apparently built into the camera electronics, and by the fact, that the camera was equipped with a Bayer-pattern sensor with different color filters in front of neighboring pixels.

Radial Profile-based Segmentation Technique

The major task in hemispheric image analysis for solar radiation measurement is the segmentation of the images with the goal of detecting open sky areas. Segmentation routines have always been a central point of research and discussion in hemispheric image processing for solar radiation analysis (Leblanc *et al.*, 2005; Jonckheere *et al.*, 2005; Wagner and Hagemeier, 2005). A segmentation technique should be independent of the type and density of the forest stand and of the sky cover. Sub-pixel classification (i.e., the quantitative detection of pixels partly containing open sky) may become crucial if the precision potential of the methods has to be optimized to allow for reliable measurements in dark forest regions with an open sky area of only 2 to 5 percent.

Early segmentation techniques were based on simple thresholding in grayscale imagery with the threshold set interactively. These techniques have the disadvantage that reasonable results can only be obtained when the weather conditions match certain criteria. In most cases, a bright homogeneously clouded sky is required. This prerequisite may considerably reduce the number of days in a year which are appropriate for taking images. Attempts with standard pixel- or segment-based multispectral classification techniques from commercial image processing software packages

TABLE 2. CHANNEL-VARIANT RADIAL DISTORTION PARAMETERS FOR TWO DIFFERENT FISHEYE LENSES (SCHWALBE AND MAAS, 2006)

Fisheye lens	Nikkor 8mm f/2.8			Sigma 8mm F4 EX		
	red	green	blue	red	green	blue
Color channel						
A1	$-5.9 \cdot 10^{-4}$	$-6.2 \cdot 10^{-4}$	$-6.2 \cdot 10^{-4}$	$-5.8 \cdot 10^{-4}$	$-6.2 \cdot 10^{-4}$	$-6.3 \cdot 10^{-4}$
A2	$1.0 \cdot 10^{-6}$	$1.4 \cdot 10^{-6}$	$1.5 \cdot 10^{-6}$	$-2.7 \cdot 10^{-6}$	$3.9 \cdot 10^{-6}$	$6.0 \cdot 10^{-6}$
A3	$-3.0 \cdot 10^{-9}$	$-4.8 \cdot 10^{-9}$	$-5.2 \cdot 10^{-9}$	$-4.1 \cdot 10^{-9}$	$-6.0 \cdot 10^{-9}$	$-6.8 \cdot 10^{-9}$
Max. difference red/green	2.57 pixel			3.25 pixel		
Max. difference blue/green	0.59 pixel			0.22 pixel		

may lead to relatively poor results (Jonckheere *et al.*, 2005). This can be attributed to the special characteristics of Bayer pattern digital camera hemispheric RGB images with rather little uncorrelated color information and an excess of mixed pixels. In addition, varying intensity of partly clouded sky complicates parameter setting in conventional segmentation techniques. Leblanc *et al.* (2005) used a two-value thresholding, allowing for a sub-pixel segmentation, which was first established in hemispherical canopy photography by Olsson *et al.* (1982) and further developed by Wagner (2001) for scanned analogue photography. Recently, Ishida (2004) proposed an automatic thresholding technique with the goal of deriving a scalar value called "diffuse site factor," and Nobis and Hunziker (2005) showed a technique for deriving a scalar "canopy openness" parameter. Jonckheere *et al.* (2004) suggested including above-canopy reference light measurement and weather conditions. Wagner and Hagemeier (2005) could show that even in this case, there is no segmentation technique available that fulfills all requirements of a flexible use of hemispherical canopy photography, e.g., LAI estimations and characterization of radiation regimes, simultaneously. Jonckheere *et al.* (2005) published advanced automatic methods for segmentation, which deliver a view angle dependent non-scalar result. However, the technique has not been validated by radiation measurements with sensors and is still prone to some subjective influences by the user.

Therefore, the goal of the work to be presented in the following sub-sections was to develop a method which allows for a reliable automatic sub-pixel segmentation of hemispheric forest crown imagery and which is suited to be used at different weather conditions and in different types of forest stands. The developed procedure can be divided into two steps. First, the pixels that purely represent the classes' sky or vegetation are determined. This is done by analyzing radial intensity profiles on the homogeneity of neighboring pixels. In addition to this texture criterion, the multispectral information is considered only for pixels, which can be identified unambiguously as a pure vegetation pixel by their RGB-values. In a second step, the remaining unclassified pixels are fully or partially assigned to one of these two classes. Mixed pixels are characterized by the percentage of the pixel in the two classes. As a result, a gray value image is obtained wherein a gray value of 255 represents pure sky pixels, and a gray value of 0 represents pure vegetation pixels. The remaining mixed pixels are gray value coded

linearly corresponding to their percentage of the class sky. The procedure is explained in detail in the following.

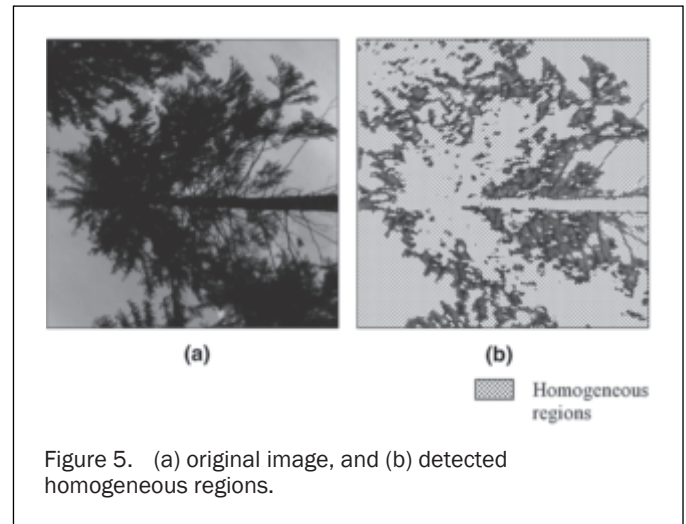
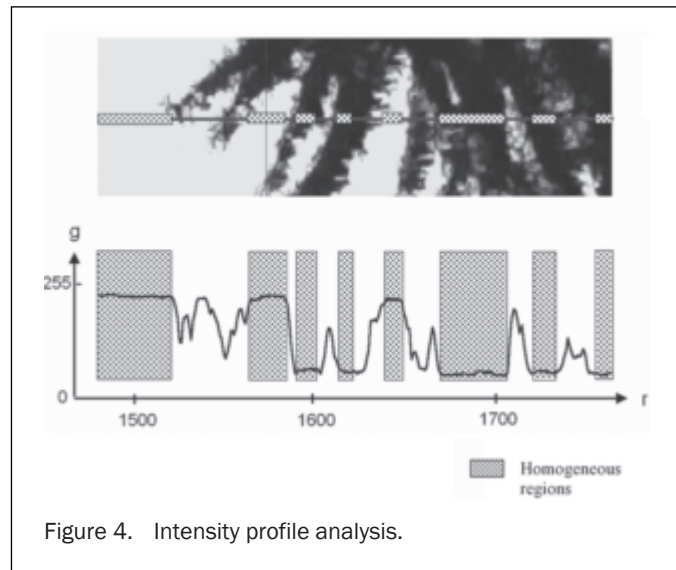
Multispectral Classification

In a first processing step, a pixel-wise multi-spectral classification is performed on the RGB image information after chromatic aberration correction. The classification is based on the intensity ratio between the blue channel and the red and green channel. Only pixels with a clear dominance of the blue channel are classified as sky. This step produces relatively few unambiguously classified pixels. The major limiting factor here is the variation in the cloudiness of the sky. Another limitation comes from the color quality of Bayer-pattern single-chip images, which have different color filters in front of neighboring pixels and generate an RGB image by interpolation techniques.

Detection of Homogeneous Regions

The characteristics of hemispherical images require local segmentation methods rather than global methods. The developed method makes use of the fact that the image is a back lighted shot. On the first view, this fact is disadvantageous because of the lack of useful color information, but on the other hand, it may be advantageous concerning the use of texture information. Therefore, the following considerations are based on the intensity values of the pixels which are calculated as mean of the pixels RGB values. Open sky areas are mostly characterized by the local homogeneity of their pixel values. In the hemispherical back lighted images the vegetation areas are also relatively homogeneous. Neighboring pure vegetation pixels will usually show small gray value differences. This means that in a first step, homogeneous regions can be detected in the images, independent on their class assignment. Inhomogeneous regions will often be transition areas between the two classes.

For the determination of homogeneous regions of the image, a profile analysis is performed. The profiles are defined radiating from the principle point of the hemispheric image. Radial profiles seem self-evident when processing fisheye images. They show the advantage of following the direction of the tree trunks and crossing most branches orthogonally. A linear filter mask (with a typical width of seven pixels) is shifted along each profile, assigning pixels to a homogeneous region if the intensity variation within the mask does not exceed a preset threshold (Figure 4). The result for a section of an image after profile-based texture analysis is shown in Figure 5.



As one can see from Figure 5, a large number of pixels are assigned to homogeneous regions by the procedure as described above. In a second step, the homogeneous regions have to be classified. After this, the remaining pixels are fully or partially assigned to one of the two classes.

Classification of Homogeneous Regions

The homogeneous segments resulting from the profile-based texture analysis cannot be classified purely based on their average intensity. Especially in the case of dark clouded sky or scattered cumulus clouds, a local approach has to be chosen.

The chosen approach is based on two threshold values and a segment neighborhood analysis. An upper and a lower global threshold, defining regions which can clearly be assigned to one of the two classes, are obtained from a smoothed intensity histogram of the homogeneous regions. Pixels in the region between the two thresholds may belong to either one of the two classes and have to be treated separately in a local approach.

Upper and lower thresholds are obtained from an analysis of the histogram of the detected homogeneous regions (Figure 6) in a process described in more detail in (Schwalbe *et al.*, 2006). Pixels with intensity values higher than the upper threshold are assigned to the class "sky"; pixels with intensity values lower than the lower threshold are assigned to the class "vegetation."

Pixels with intensity values in the range between the two thresholds cannot be assigned to one of the two classes globally. Instead, the remaining unclassified regions are assigned to one of the two classes based on a local analysis using their unambiguously classified neighboring regions. For this purpose the neighborhood of each unclassified pixel is spirally scanned until a sufficient number of pixels (e.g., 30 pixels) that belong to the class sky as well as of pixels that belong to the class vegetation are found (see Figure 7). The intensity value of the unclassified pixel is now compared to the average intensity values (reference values) of these already classified neighbor pixels. The unclassified pixel is then assigned to the class with the lower intensity value difference. As a result of this processing step, all pixels belonging to the homogeneous regions are classified.

The spiral search may be rather time consuming. In order to save computation time, the strict spiral search may optionally be performed only to a thinned subset of the unclassified pixels, transferring the local class reference intensity value information to neighboring unclassified pixels.

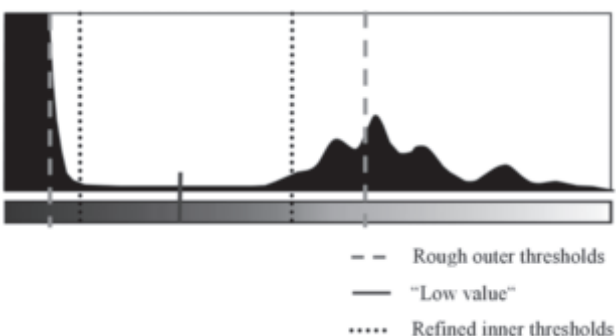


Figure 6. Homogeneous regions histogram analysis.

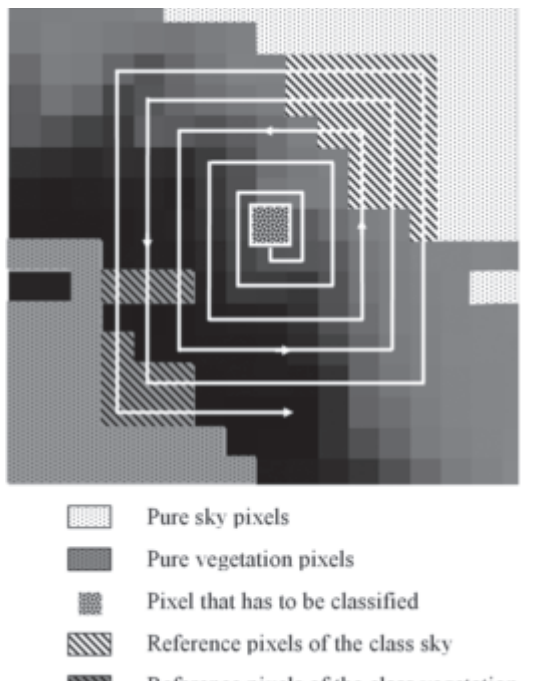


Figure 7. Spiral search for reference values.

An example of the result of the global and local classification step is shown in Figure 8.

Sub-pixel Classification of Mixed Pixels

In the last processing step, all pixels which could not be classified unambiguously on the basis of their RGB-information or assigned to homogeneous regions, have to be classified. As these inhomogeneous region pixels may be mixed pixels partially belonging to both classes, a sub-pixel classification has to be performed here. This sub-pixel classification is again achieved by a local search for reference pixels, which are clearly assigned to one class. A pixel is partly assigned to both classes, with the membership percentage obtained by linear interpolation of the intensity value of the pixel between the local reference values of the two classes, which are detected in a spiral search procedure as previously shown (Figure 7). If the intensity of a mixed pixel I_{pix} is higher than or equal to its local reference value of the class sky (I_{sky}), it is assigned to the class "sky" with a percentage of 100 percent. If it is lower than or equal to its reference value of the class vegetation (I_{veg}), it is assigned to the class "sky" with a percentage of 0 percent. If the intensity value is between the two local reference values, the assignment percentage to the class "sky" is:

$$P_{sky} = 100 \cdot (I_{pix} - I_{veg}) / (I_{sky} - I_{veg}). \quad (6)$$

Figure 9 shows an example of a result of the combined sub-pixel classification process with the assignment percentage scaled to gray values 0 ... 255.

The method allows for a reliable classification of hemispherical images taken at different weather conditions. A special situation occurs when the sky is scattered clouded. In this case, misclassifications can sometimes appear at the margins of the clouds. The reason is that pixels located there are detected as inhomogeneous pixels.

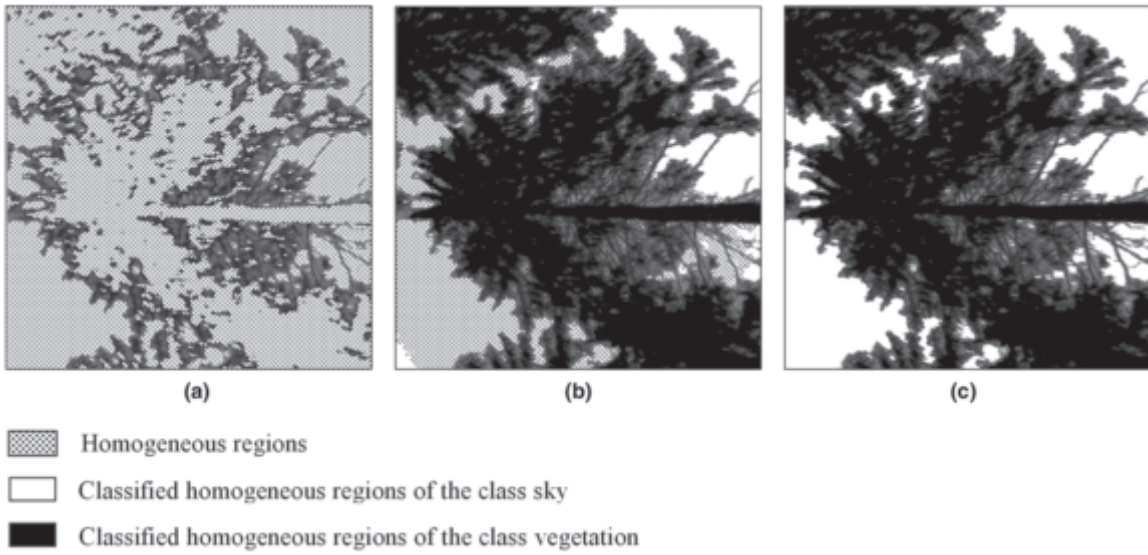


Figure 8. (a) detected homogeneous regions, (b) regions classified by global thresholding, and (c) completely classified homogeneous regions.

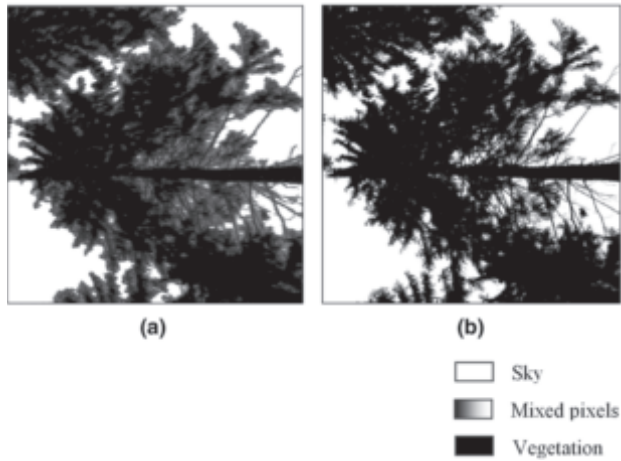


Figure 9. (a) classified homogeneous regions, and (b) grey value coded mixed pixels.

These pixels are then treated as mixed pixels and classified as explained above. Due to strong intensity differences between blue sky and bright clouds, wrong reference values are found in some cases. This means that the accordant mixed pixel is not classified as sky but obtains a slightly lower gray value (Figure 10).

Computation of Solar Radiation Measures

The resulting segmented and classified image can be used as input to the solar radiation calculation algorithm. The image shows crown gap regions, through which solar radiation can reach a growing plant. The general assumption of the radiation model is that canopy openings are transparent and foliage is opaque for solar radiation (Rich,

1990), neglecting any scattered light. A diffuse site factor is calculated, which is defined as the percentage of diffuse light at a given site on the ground compared to the total light above the canopy (Anderson, 1964). Based on a standard solar track, the solar radiation penetration (global radiation and photosynthetic active radiation) can be calculated as a function of time of the year and time of the day (Evans and Coombe, 1959; Smith and Somers, 1993). The value consists of diffuse skylight and direct sunlight rated after local portions of cloudiness. The different relevance of light reaching the plant from the zenith or from close to the horizon is also considered in the model.

Practical Results

The validation of the results of hemispherical image processing was performed by using PAR-sensors, which are sensitive to a wavelength between 400 nm and 700 nm. Ten sensors were systematically positioned over four different forest sites (Table 3) during the main vegetation period over three years. The stand densities vary between low (0.4° stocking degree) and high (1.0° stocking degree), and accordingly more or less light can pass through the canopy to the bottom. The sensors remained in their position integrating measurements for a minimum of four weeks. Their positions were marked to warrant alignment of the hemispherical photographs to be taken the same positions. The radiation above the canopy was measured with the same type of sensor on the top of a measuring tower at 40 m height.

The ten PAR sensors took measurements (in $\mu\text{mol}/\text{m}^2/\text{s}$) in intervals of 30 seconds. The canopy top reference sensor had measuring intervals of one minute. The measurements of all PAR sensors were integrated to 10 minute averages. To be able to compare the radiation value calculated from the photo (which should be independent on the cloudiness) to the reference radiation value measured by the sensor (which is affected by cloudiness), the weather condition during the sensor measurement has to be



Figure 10. Classified hemispherical image with scattered clouded sky.

TABLE 3. DESCRIPTION OF STUDY SITE, STANDS, AND WEATHER CONDITIONS WHILE TAKING IMAGES

Stand	1	2	3
Coordinates	50°58'N 13°34'E	50°57'N 13°29'E	50°58'N 13°30'E
Species	<i>Picea abies</i>	<i>Picea abies</i>	<i>Picea abies</i>
Stocking degree (stand density)	0.4°, 0.6°, 0.8°	0.3°–1.2°	0.5°–0.9°
Mean Diameter (breast height) (cm)	33 ± 2	28 ± 5	29 ± 3
Average tree height (m)	28 ± 3	25 ± 4	27 ± 3
Cloudiness condition	70 to 90% clouds	70 to 90% clouds	70 to 90% clouds
Wind velocity (Beaufort)	<2	<2	<2

TABLE 4. OVERVIEW OF TEST CONDITIONS OF THE VALIDATION METHOD; THE "CLOUDINESS FACTOR" REFERS TO THE PORTION OF THE INDICATED TIME PERIOD AT WHICH CLOUDS OBSTRUCTED THE HEMISPHERE (WAGNER, 1996)

Area	Stand density	Time period	Number of Days	Cloudiness factor
1	Low to high	29.06.-04.09.2006	67	0.76
2	High	22.07.-18.08.2004	27	0.36
3a	Middle to high	13.05.-06.07.2005	53	0.54
3b	High	29.04.-26.06.2006	58	0.70

considered. A cloudiness factor (Table 4), obtained from a comparison with the calculated PAR-data of an open air hemispherical image with the canopy top PAR sensor, is used for normalizing the ground PAR sensor measurements (Wagner, 1996).

The hemispherical photographs were processed with the solar radiation model to calculate the photosynthetic active radiation of each position at intervals synchronized to the PAR sensor measurements (Wagner, 1996). Figure 11 shows results for all 40 sensor positions, comparing the results of hemispheric image processing to the PAR sensor measurements after cloudiness correction. The different stand densities are clearly recognizable from the PAR values ranging from 5 percent to 40 percent of the radiation above the canopy. Both methods for estimation of solar radiation in forest stands show similar results, which are comparable with studies from Ishida (2004) and Nobis and Hunzicker (2005). The data match especially well in the dark stands

(below 10 percent), which turned out to be most critical in former studies.

Conclusions

It could be shown that the precision, reliability, and flexibility of hemispheric forest crown image processing can be improved significantly by the consequent application of photogrammetric sensor modeling and image analysis techniques. Applying an equi-angular camera model with additional parameters transferred from central perspective camera modeling, an precision of 0.1 pixel in image space could be obtained for low-cost off-the-shelf fisheye lenses. Chromatic aberration has to be taken into account if color images generated by a fisheye lens are being processed. Hemispheric forest crown image segmentation techniques could be improved by combining local and global analysis and exploiting the characteristics of hemispheric forest

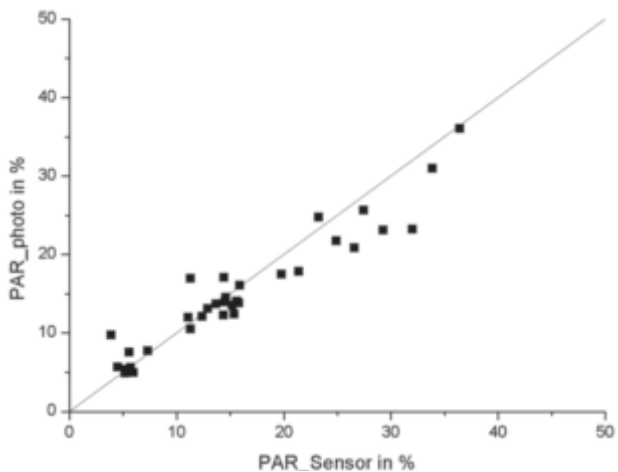


Figure 11. PAR-value in percentage of sensor versus PAR-value in percentage of hemispherical photographs (study sites and conditions are described in Table 3).

crown images. As a result, the accuracy and flexibility of applying hemispheric photography in solar radiation determination for silvicultural analysis in forest ecosystems could be enhanced significantly.

The camera modeling and segmentation routines developed here offer all those features, which silviculture scientists have been looking for in the last years: The method delivers spatially resolved results, it is not affected by subjective operator influence and it is robust against different conditions of cloudiness. The fact that segmentation is performed at subpixel-level leads to satisfying results even in critical dark environments (Figure 12) with relative radiation levels of less than 10 percent of open field.

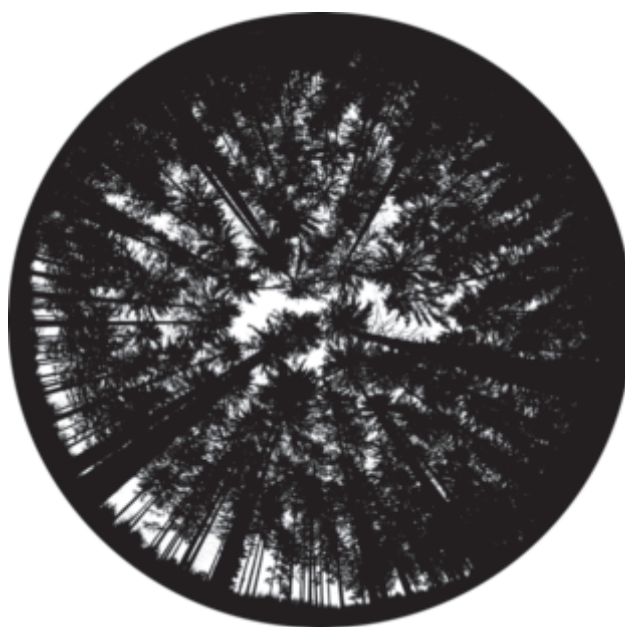


Figure 12. Classified hemispherical image of a dense forest stand.

Acknowledgments

The work presented in the paper was supported by DFG (Deutsche Forschungsgesellschaft - German Research Foundation) under grant number WA 1515/6.

References

- Anderson, M.C., 1964. Studies of the woodland light climate, *Journal of Ecology*, 52:27–41.
- Bonhomme, R., and P. Chartier, 1972. The interpretation and automatic measurement of hemispherical photographs to obtain sunlit foliage area and gap frequency, *Israel Journal of Agricultural Resources*, 22(2):53–61.
- Brown, D., 1971. Close-range camera calibration, *Photogrammetric Engineering*, 37(8):855–866.
- Burschel, P., and J. Schmaltz, 1965. Die Bedeutung des Lichtes für die Entwicklung junger Buchen, *Allgemeine Forst - u.Jagd-Zeitung*, 136(9):193–210.
- Chen, J.M., T.A. Black, and R.S. Adams, 1991. Evaluation of hemispherical photography for determining plant area index and geometry of a forest stand, *Agricultural and Forest Meteorology*, 56:129–143.
- Clearwater, M.J., T. Nifinluri, and P.R. van Gardingen, 1999. Forest fire smoke and a test of hemispherical photography for predicting understorey light in Bornean tropical rain forest, *Agricultural and Forest Meteorology*, 97:129–139.
- Dohrenbusch, A., 1989. Die Anwendung fotografischer Verfahren zur Erfassung des Kronenschlussgrades, *Forstarchiv*, Jg., 60:151–155.
- El-Hakim, S.F., 1986. Real-time image metrology with CCD Cameras, *Photogrammetric Engineering & Remote Sensing*, 52(11):1757–1766.
- Englund, S.R., J.J. O'Brien, and D.B. Clark, 2000. Evaluation of digital and film hemispherical photography and spherical densitometry for measuring forest light environments, *Canadian Journal of Forest Research*, 30:1999–2005.
- Evans, G.C., and D.E. Coombe, 1959. Hemispherical and woodland canopy photography and the light climate, *Journal of Ecology*, 47:103–113.
- Ishida, M., 2004. Automatic thresholding for digital hemispherical photography, *Canadian Journal of Forest Research*, 34:2208–2216.
- Jonckheere, I., S. Fleck, K. Nackaerts, B. Muys, P. Coppin, M. Weiss, and F. Baret, 2004. Review of methods for in situ leaf area index determination - Part I. Theories, sensors, and hemispherical photography, *Agricultural and Forest Meteorology*, 121:19–35.
- Jonckheere, I., K. Nackaerts, B. Muys, and P. Coppin, 2005. Assessment of automatic gap fraction estimation of forests from digital hemispherical photography, *Agricultural and Forest Meteorology*, 132:96–114.
- Leblanc, G., J. Chen, R. Fernandes, D. Deering, and A. Conley, 2005. Methodology comparison for canopy structure parameters extraction from digital hemispherical photography in boreal forests, *Agricultural and Forest Meteorology*, 129:187–207.
- Luhmann, T., H. Hastedt, and W. Tecklenburg, 2006. Modelling of chromatic aberration for high precision photogrammetry, *Proceedings of the ISPRS Commission V Symposium: Image Engineering and Vision Metrology, International Archives of Photogrammetry and Remote Sensing*, 36(5):173–178.
- Nobis, M., and U. Hunziker, 2005. Automatic thresholding for hemispherical canopy photographs based on edge detection, *Agricultural and Forest Meteorology*, 128:243–250.
- Olsson, L., K. Carlsson, H. Grip, and K. Perttu, 1982. Evaluation of forest-canopy photographs with diode-array scanner OSIRIS, *Canadian Journal of Forest Research*, 12:822–828.
- Pacala, S.W., C.D. Canham, A.J. Silander Jr., and R.K. Kobe, 1994. Sapling growth as a function of resources in a north temperate forest, *Canadian Journal of Forest Research*, 24:2172–2183.
- Ray, S.F., 1994. *Applied Photographic Optics: Lenses and Optical Systems for Photography, Film, Video and Electronic Imaging*, Second edition, Oxford: Focal Press, pp. 559–563.

- Rich, P.M., 1990. Characterizing plant canopies with hemispherical photographs, *Remote Sensing Reviews*, Harwood Academic Publishers, 5(1)107–127.
- Schneider, D., and H.-G. Maas, 2006. A geometric model for linear array based terrestrial panoramic cameras, *The Photogrammetric Record*, 21(115):198–210.
- Schwalbe, E., 2005. Geometric modelling and calibration of fisheye lens camera systems, *Proceedings of the 2nd Panoramic Photogrammetry Workshop, International Archives of Photogrammetry, Remote Sensing and Spatial Information Sciences* (R. Reulke and U. Knauer, editors), Vol. XXXVI, Part 5/W8.
- Schwalbe, E., and D. Schneider, 2005. Design and testing of mathematical models for a full-spherical camera on the basis of a rotating linear array sensor and a fisheye lens, *Optical 3D Measurement Techniques VII* (A. Grün and H. Kahmen, editors), Vol. I, pp. 245–254.
- Schwalbe, E., and H.-G. Maas, 2006. Ein Ansatz zur Elimination der chromatischen aberration bei der modellierung und kalibrierung von fisheye-aufnahmesystemen, *Photogrammetrie - Laserscanning - Optische 3D-Messtechnik*, Beiträge Oldenburger 3D-Tage 2006, Hrsg. Th. Luhmann, Verlag Herbert Wichmann.
- Schwalbe, E., H.-G. Maas, M. Kenter, and S. Wagner, 2006. Profile based sub-pixel-classification of hemispherical images for solar radiation analysis in forest ecosystems, *Proceedings of ISPRS Commission VII Symposium*, Enschede, The Netherlands, unpaginated CD-ROM.
- Smith, W.R., and G.L. Somers, 1993. A system for estimating direct and diffuse photosynthetically active radiation from hemispherical photographs, *Computers and Electronics in Agriculture*, 8:181–193.
- van den Heuvel, F.A., R. Verwaal, and B. Beers, 2006. Calibration of fisheye camera systems and the reduction of chromatic aberration, *ISPRS Commission V Symposium: Image Engineering and Vision Metrology*, unpaginated CD-ROM.
- Wagner, S., 1996. Übertragung strahlungsrelevanter Wetterinformation aus punktuellen PAR-Sensordaten in größere Versuchsflächenanlagen mit Hilfe hemisphärischer Fotos, *Allgemeine Forst- u.Jagd-Zeitung*, 167(1/2):34–40.
- Wagner, S., 1998. Calibration of grey values of hemispherical photographs for image analysis. *Agricultural and Forest Meteorology*, 90(1/2):103–117.
- Wagner, S., 2001. Relative radiance measurements and zenith angle dependent segmentation in hemispherical photography, *Agricultural and Forest Meteorology*, 107(2):103–115.
- Wagner, S., and M. Hagemeier, 2005. Method of segmentation affects leaf inclination angle estimation in hemispherical photography, *Agricultural and Forest Meteorology*, 139:12–24.
- Zhang, Y., J.M. Chen, and J.R. Miller, 2005. Determining digital hemispherical photograph exposure for leaf area index estimation, *Agricultural and Forest Meteorology*, 133:166–181.

(Received 27 April 2007; accepted 19 July 2007; revised 14 December 2007)